
This is the **accepted version** of the journal article:

Wang, Zhuopeng; Ananias, Duarte; Carné-Sánchez, Arnau; [et al.]. «Lanthanide-organic framework nanothermometers prepared by spray-drying». Advanced functional materials, Vol. 25, Issue 19 (May 2015), p. 2824-2830. DOI 10.1002/adfm.201500518

This version is available at <https://ddd.uab.cat/record/307872>

under the terms of the  ^{IN}
COPYRIGHT license

Lanthanide organic framework nanothermometers prepared by spray-drying

by Zhuopeng Wang, Duarte Ananias, Arnau Carné-Sánchez, Carlos D. S. Brites, Inhar Imaz, Daniel Maspoch, João Rocha and Luís D. Carlos**

Dr. Z. Wang, Dr. D. Ananias, Dr. C. D. S. Brites, Prof. Dr. J. Rocha and Prof. Dr. L. D. Carlos
Departments of Chemistry and Physics, CICECO, University of Aveiro, 3810-193 Aveiro, Portugal
E-mail: rocha@ua.pt (J.R.) lcarlos@ua.pt (L.D.C.)

Dr. A. Carné-Sánchez, Dr. I. Imaz, and Prof. Dr. D. Maspoch
ICN2 (ICN-CSIC), Institut Català de Nanociència i Nanotecnologia, Esfera UAB, 08193 Bellaterra, Spain

Prof. Dr. D. Maspoch
Institució Catalana de Recerca i Estudis Avançats (ICREA), 08100 Barcelona, Spain

Keywords: MOFs, lanthanide ions, spray-drying, luminescence, nanothermometers

Abstract:

The accurate, non-invasive and self-referenced temperature measurement at the submicron scale is of great interest, prompted by the ever-growing demands in the fields of nanotechnology and nanomedicine. The thermal dependence of the phosphor's luminescence provides high detection sensitivity and spatial resolution with short acquisition times in, e.g. biological fluids, strong electromagnetic fields and fast-moving objects. Here, we show that nanoparticles of $[(\text{Tb}_{0.914}\text{Eu}_{0.086})_2(\text{PDA})_3(\text{H}_2\text{O})]\cdot 2\text{H}_2\text{O}$ (PDA=1,4-phenylenediacetic acid), the first lanthanide-organic framework prepared by the spray-drying method, are excellent nanothermometers operating in the solid state in the 10 to 325 K range (quantum yield of 0.25 at 370 nm, at room temperature). Intriguingly, this system is the most sensitive cryogenic nanothermometer reported so far, combining high sensitivity (up to $5.96 \pm 0.04 \text{ \%}\cdot\text{K}^{-1}$ at 25 K), reproducibility (in excess of 99%) and low-temperature uncertainty (0.02 K at 25 K).

1. Introduction

Precise temperature measurement at the submicron scale is an important challenge encountered, namely, in the fields of nanotechnology and nanomedicine.^[1] Thermometers working in an accurate, non-invasive way and with a high spatial resolution are critical to monitoring numerous processes at the microscale and nanoscale within electronic and photonic devices, such as thermal transport, heat dissipation and thermal reactions.^[2] As a recently emerged non-invasive technique, the thermal dependence of the phosphor's luminescence provides a high detection sensitivity and spatial resolution, with short acquisition times, in biological fluids, strong electromagnetic fields and fast-moving objects, for which the conventional methods are ineffective. To fulfill the great potential of this technique, the discovery of new materials with tuneable luminescence is very important and has recently become an active research area. Among phosphors, such as organic dyes,^[3] polymers,^[4] semiconductor nanocrystals,^[5] lanthanide (Ln)-based materials are the most versatile thermal probes used in luminescent nanothermometers.^[6] Several examples of such materials demonstrating their application in sensing or mapping at the sub-micron scale were reported: Er³⁺/Yb³⁺ co-doped fluoride glass^[7] or PbF₂ nanoparticles,^[8] glued at the extremity of an atomic force microscope scanning tip, NaYF₄:(Er³⁺,Yb³⁺)^[9] and Ln-doped NaGdF₄ core-shell nanoparticles;^[10] Y₂O₃:Eu³⁺,^[11] Y₃Al₅O₁₂:Ce³⁺ ^[12] and Mo sensitized rare-earth oxide nanoparticles;^[13] and siloxane-based nanoparticles incorporating a Eu³⁺ tris(β-diketonate) complex.^[14] The temperature determination is usually based on the change of the luminescence intensity or decay-times. However, the measurements based on a single f-f transition may be much affected by the variation of the sensor concentration and the drift of the optoelectronic systems namely, the excitation sources and detectors. Recently, Carlos *et al.*, reported self-reference nanothermometers based on the intensity ratio of two f-f transitions that overcome the drawbacks of temperature determination with a single-transition.

Metal-organic frameworks (MOFs) are crystalline materials consisting of well-defined networks formed by the self-assembly of metal cations and organic linkers. The luminescence properties of MOFs have attracted attention due to the unique hybrid networks of these materials, in which both the inorganic and organic moieties may be optically-active, enabling a wide range of emissive phenomena found in few other classes of materials.^[16] Moreover, the occurrence of distinctive processes, such as metal-ligand charge-transfer and host-guest interactions^[16a] along with the ease of modification (*e.g.*, doping in composition^[17]) provide a wealth of opportunities for engineering luminescence properties. In the past two decades, luminescent MOFs have found potential applications in chemical sensing, light-emitting devices, and biomedicine.^[16, 18] The use of luminescent MOF nanoparticles in sensing, biomedical imaging and drug delivery is also well documented.^[19] Cui *et al.* reported the first ratiometric luminescent MOF thermometer, $\text{Eu}_{0.0069}\text{Tb}_{0.9931}\text{-DMBDC}$ (DMBDC = 2,5-dimethoxy-1,4-benzenedicarboxylate), based on the emissions of Tb^{3+} at 545 nm and Eu^{3+} at 613 nm.^[20] Recently, the same group suggested a new type of ratiometric thermometer that combines the Eu^{3+} emission of a MOF ($\text{Eu}_2(\text{QPTCA})(\text{NO}_3)_2(\text{DMF})_4 \cdot (\text{CH}_3\text{CH}_2\text{OH})_3$, QPTCA = 1,1':4',1'':4'',1''':4''',1''''-quaterphenyl-3,3''',5,5'''-tetracarboxyl, and DMF = dimethylformamide) hosting a perylene dye in the pores.^[21] The resulting MOF \supset dye thermometer makes use of the dye/ Eu^{3+} emission intensity ratio to measure the temperature in the physiological range, with a maximum sensitivity of $1.28\% \cdot \text{K}^{-1}$ at 293 K. The only report available on a Ln-MOF ratiometric nanothermometer describes nanoparticles prepared by reverse emulsion, showing an excellent performance in the physiological temperature range, thus holding considerable potential as nanoplatforms for biological and biomedical applications.^[22]

The synthesis of MOF nanoparticles is still a challenging task, despite many attempts and several proposed strategies including coordination modulation, ultrasonic-, microwave-, interfacial- and ionic liquid/microemulsion-synthesis.^[23] Maspoch *et al.*^[24] and Marquez *et al.*^[25] reported approaches capable of affording a wide range of nanosized MOFs based on the

spray-drying method: the reaction medium is atomized into droplets and MOF nanoparticles form during the drying process and self-assemble into superstructures within the droplets, which act as individual reactors confining the growth of the crystals. This method is attractive because it emulates the microemulsion synthesis, restraining the reagents to the droplets, without using a secondary immiscible solvent. Thus, the method reduces the synthesis complexity and, most importantly, it enables scaling-up the production of MOF nanoparticles. Here, we show that spray-drying prepared MOF nanoparticles of $[(\text{Tb}_{0.914}\text{Eu}_{0.086})_2(\text{PDA})_3(\text{H}_2\text{O})]\cdot 2\text{H}_2\text{O}$ (PDA = 1,4-phenylenediacetic acid), denoted as $\text{Tb}_{0.914}\text{Eu}_{0.086}\text{-PDA}$, may be used as ratiometric luminescent nanothermometers operative over a wide range of temperatures, in particular, in the cryogenic range. The luminescence features of the bulk and nanosized material are discussed.

2. Results and Discussion

The use of 1,4-phenylenediacetic acid in the synthesis of $\text{La}^{3+}/\text{Er}^{3+}$ -MOFs was first reported by Pan *et al.*^[26] The syntheses were further extended to all Ln elements, except for Pm and Lu, affording a series of thermally stable (up to 723 K) isostructural MOFs (Ln-PDA).^[27] In the structure of Ln-PDA, the Ln^{3+} ions are interconnected through COO^- groups, forming a Ln- COO^- triple-helix chain along the *c* direction. These helices are cross-linked by the $-\text{CH}_2\text{C}_6\text{H}_4\text{CH}_2-$ groups of the PDA anions, generating an extended three-dimensional network with one-dimensional channels, hosting the coordinated water molecules.^[26-27]

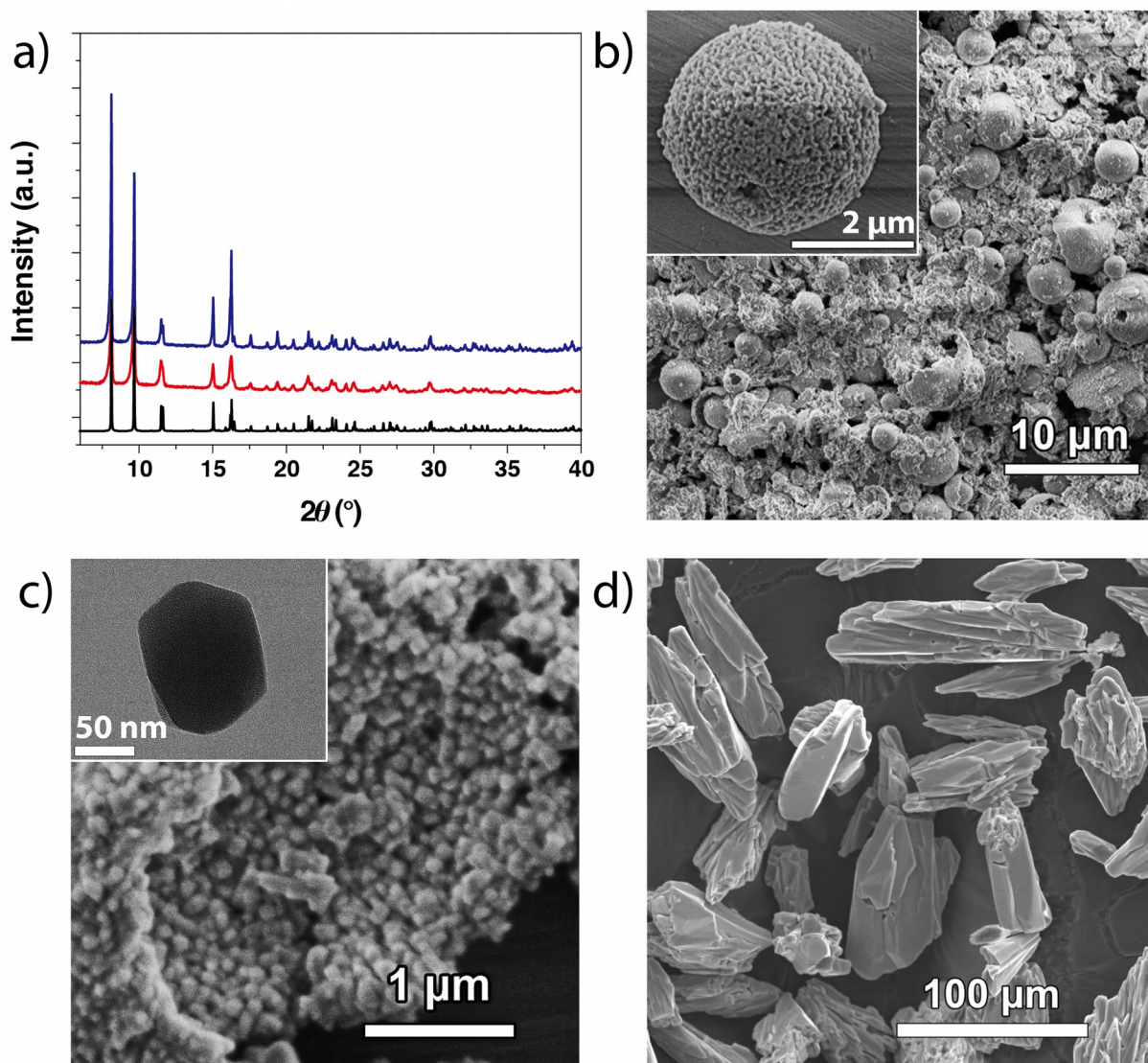


Figure 1. a) Experimental powder X-ray diffraction patterns of spray-drying prepared $\text{Tb}_{0.914}\text{Eu}_{0.086}\text{-PDA}$ (red) and bulk (blue) MOFs; the simulated pattern is depicted in black; b) Scanning electron microscopy (SEM) images of spray-drying prepared MOF; the inset shows a single spherical aggregate; c) SEM image of a crushed shell showing the hollow structure of the spray-drying particles; the inset depicts a TEM image of a crystal isolated from the aggregate by sonication; d) SEM image of the bulk MOF prepared by solvothermal synthesis.

Mixed $\text{Tb}^{3+}/\text{Eu}^{3+}$ MOF nanoparticles were obtained by the spray-drying method and, to the best of our knowledge, this is the first report on using this technique for preparing Ln-bearing MOFs. The bulk counterpart was also synthesized, for comparison, and the materials have the formula $[(\text{Tb}_{1-x}\text{Eu}_x)_2(\text{PDA})_3(\text{H}_2\text{O})]\cdot 2\text{H}_2\text{O}$, with $x = 0.086$ and 0.060 for spray-dried and bulk samples, respectively, as ascertained by induced coupled plasma spectroscopy. Powder X-ray diffraction (**Figure 1a**) indicates that the bulk and nanosized materials are pure and highly

crystalline and have the structure of Ln-PDA.^[27] Scanning electron microscopy (Figure 1b) shows that the spray-dried product consists of spherical superstructures of several microns, which is the typical morphology observed when using such a technique.^[24] These superstructures are hollow (Figure 1c), with a shell consisting of a thin layer of close-packing nanoparticles (210 ± 106 nm, Figure S1), and may be broken down by applying sonication or a small mechanical force (inset of Figure 1c). In contrast, the bulk particles are tens of microns in size (Figure 1d).

To understand the photoluminescence of the mixed-Ln MOFs, the Eu-PDA, Tb-PDA and Y-PDA excitation and emission spectra were studied (Figure S2). The latter was used to observe the emission of the PDA ligand in the absence of $\text{Eu}^{3+}/\text{Tb}^{3+}$, because Y^{3+} is optically inert. The excitation spectrum of Y-PDA exhibits an intense broad band at 370 nm attributed to the ligand $\pi \rightarrow \pi^*$ electronic transitions. Such a broad ligand band is not observed in the Eu-PDA and Tb-PDA excitation spectra, indicating the absence of an efficient ligand-to- Ln^{3+} energy transfer. The spectrum of Eu-PDA monitored within the $\text{Eu}^{3+} \ ^5\text{D}_0 \rightarrow \ ^7\text{F}_2$ transition exhibits a series of sharp lines assigned to the $\ ^7\text{F}_{0,1} \rightarrow \ ^5\text{D}_{0-4}$, $\ ^5\text{L}_6$, $\ ^5\text{G}_{2-6}$, $\ ^5\text{H}_{3-7}$ and $\ ^5\text{F}_{1-5}$ Eu^{3+} intra- $4f^6$ transitions (Figure S2), according to Carnall *et al.*^[28] The excitation spectrum of Tb-PDA is dominated by an intense broad band in the range 230–300 nm attributed to the spin-forbidden (high-spin, HS) interconfigurational $4f^8 \rightarrow 4f^75d^1$ transition of Tb^{3+} , while the intra- $4f^8$ transition between the $\ ^7\text{F}_6$ ground state and the $\ ^5\text{D}_{4,0}$ and $\ ^5\text{G}_J$ excited states of Tb^{3+} are weaker.

Figure 2a shows the excitation spectra of mixed-Ln MOFs at room temperature and 12 K, monitored within the $\text{Tb}^{3+} \ ^5\text{D}_4 \rightarrow \ ^7\text{F}_5$ transition (545 nm). The bands from 300 to 500 nm are given by the $\ ^7\text{F}_6 \rightarrow \ ^5\text{D}_{1-4}$, $\ ^5\text{G}_{3-6}$, $\ ^5\text{H}_7$ and $\ ^5\text{L}_{7-10}$ intraconfigurational forbidden $4f^8 \rightarrow 4f^8$ transitions of Tb^{3+} , while the broad band at 260-300 nm is assigned to the spin-forbidden (high-spin, HS) interconfigurational $4f^8 \rightarrow 4f^75d^1$ transition of Tb^{3+} . The band at ca. 245 nm is ascribed to the spin-allowed (low-spin, LS) interconfigurational fd transition of Tb^{3+} . As expected, in the mixed-Ln framework Tb^{3+} may sensitize Eu^{3+} . The excitation spectra of mixed-Ln MOFs

shown in Figure 2c and d (room temperature and 12 K) exhibit the ${}^7F_6 \rightarrow {}^5D_{1-4}$, ${}^5G_{3-6}$, 5H_7 and ${}^5L_{7-10}$ Tb^{3+} lines while monitoring at 612 nm ($Eu^{3+} {}^5D_0 \rightarrow {}^7F_2$ line), indicating a Tb^{3+} -to- Eu^{3+} energy transfer process. The 5D_0 decay curves of the spray-drying prepared sample excited at 393 (Eu^{3+} level) and 377 nm (Tb^{3+} level) display a single-exponential behaviour (Figure S3). Comparing with the 5D_0 lifetime obtained by direct excitation, the larger value obtained for the excitation via the Tb^{3+} levels (Figure S3) indicates that a second source feeds the 5D_0 level, thus providing further evidence for the Tb^{3+} -to- Eu^{3+} energy transfer.

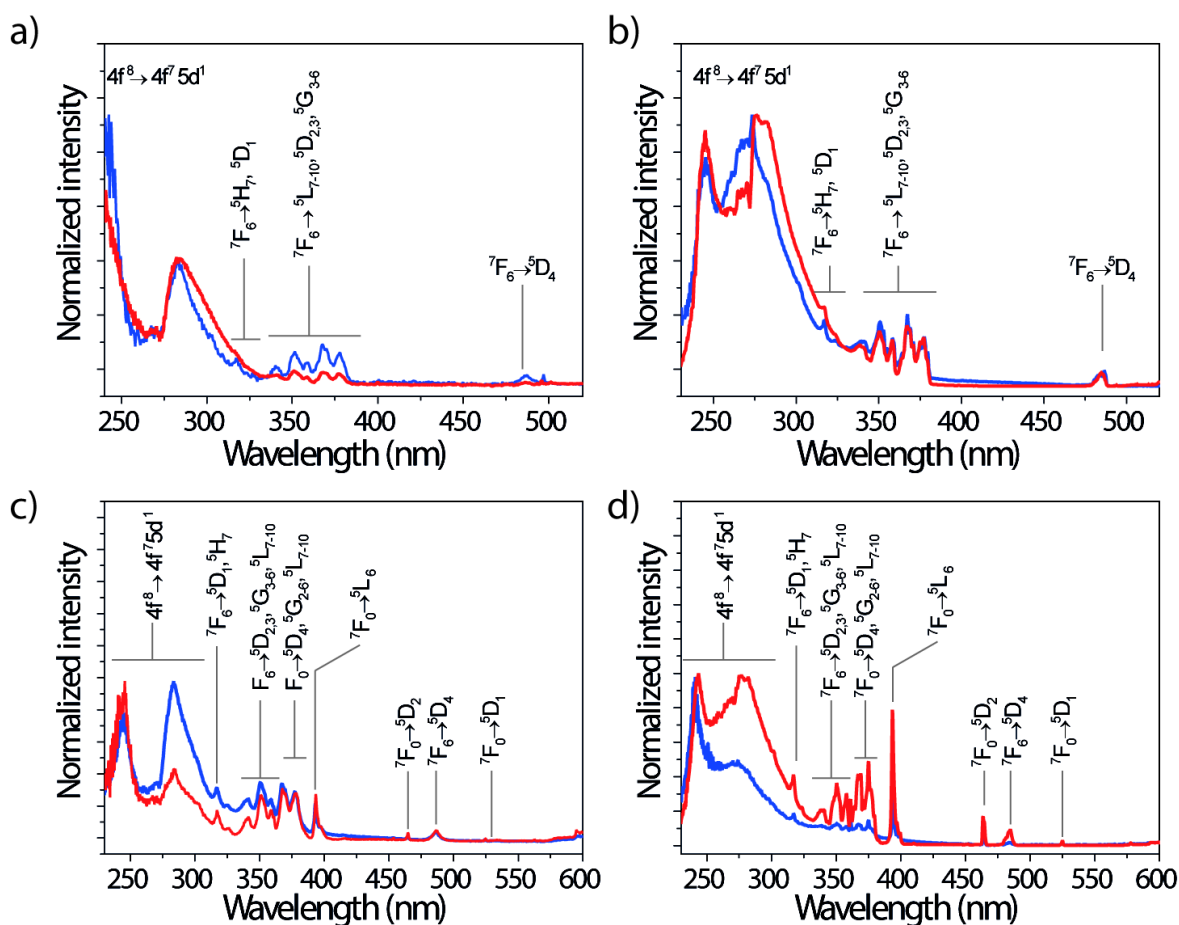


Figure 2. Excitation spectra of bulk and spray-drying prepared MOFs recorded at: a) room temperature, monitoring at 545 nm (Tb^{3+} level); b) 12 K, monitoring at 545 nm; c) room temperature, monitoring at 612 nm (Eu^{3+} level); and d) 12 K, monitoring at 612 nm. The blue and red lines depict the bulk and spray-drying prepared MOFs, respectively.

The emission spectra of the bulk and spray-dried mixed-Ln MOFs were recorded at room temperature and 12 K (**Figure 3**). All spectra exhibit the characteristic emission bands

assigned to the $^5D_4 \rightarrow ^7F_J$ ($J = 6, 5, 4$, and 3) and $^5D_0 \rightarrow ^7F_J$ ($J = 1, 2, 3$, and 4) transitions of Tb^{3+} and Eu^{3+} , respectively. Comparing with the maximum number of Stark components for each level, particularly at 12 K, it is clear that more than one independent Ln^{3+} site is present, which is consistent with the crystallographic evidence.^[27] Interestingly, the main difference between the bulk and the nanosized materials is the fact that the emission of the ligand (intense broad band at 450 nm) is observable only for the former. The broad ligand emission overlaps with the Tb^{3+} $^5D_4 \rightarrow ^7F_{6,5}$ emission transitions, thus interfering with the measurement of the Tb^{3+} luminescence intensity. Although at this point we are unable to provide a detailed explanation for this phenomenon, and considering that the two samples are identical, or very similar, in structure and chemical composition (Figure S4 and Figure S5), we submit that it is related with the different crystal size of the bulk and spray-drying materials. The absence of the ligand emission for the latter is advantageous for its application in luminescence thermometry. Moreover, the absolute emission quantum yield (exciting at 370 nm) of the nanosized MOF (0.25 ± 0.03) is larger than that of the bulk material (0.16 ± 0.02).

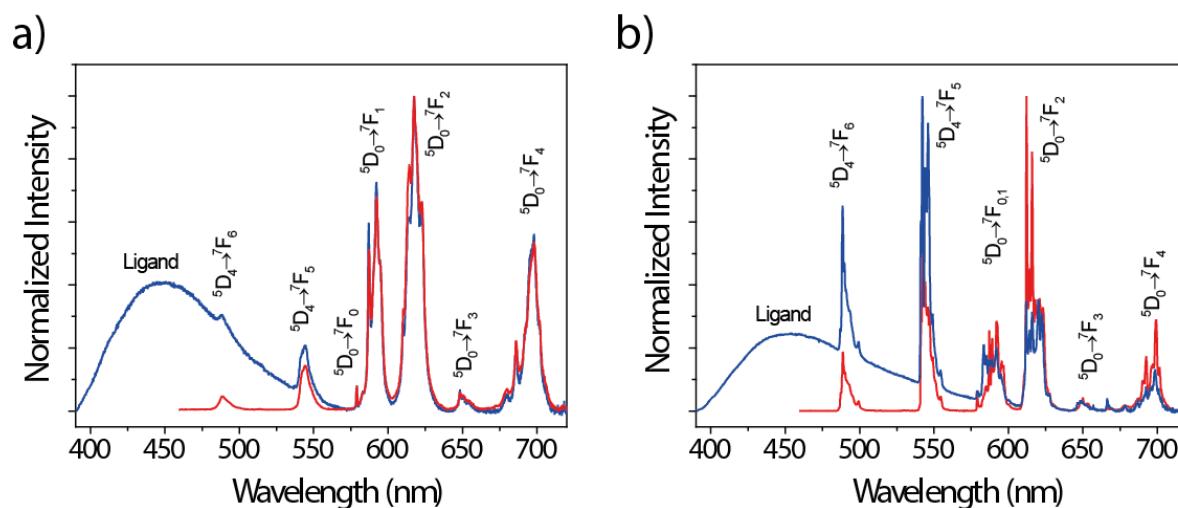


Figure 3. Emission spectra of bulk and spray-drying prepared MOFs recorded at a) room temperature, b) 12 K. The spectra were acquired with the excitation fixed at 377 nm; blue and red lines depict the bulk and spray-drying prepared MOFs, respectively.

To assess the potential of spray-drying prepared Tb_{0.914}Eu_{0.086}-PDA as a nanothermometer, its photoluminescence was investigated in 10–325 K range. Excitation at 377 nm (4f⁸ ⁵D₃ level) allows Eu³⁺ emission via a ‘conventional’ f-f energy transfer mechanism rather than f-d inter-configurational excitation (ca. 290 nm), which is more complex and requires further study. Qualitatively, the temperature may be assessed by the naked eye because the (x,y) CIE (*Commission Internationale de l’Eclairage*) 1931 color coordinates computed from the emission spectra in **Figure 4a** show a progressive evolution from the yellow, (0.510,0.458) at 10 K, to the almost pure red, (0.646,0.351) at 325 K (Figure S6 and S7). For a quantitative approach, the steady-state emission spectra show that the narrow lines of both Ln³⁺ emitting centres are temperature dependent. The thermometric parameter Δ , provides a reliable and robust method of determining the temperature, already used to map integrated circuits^[15, 29] and microfluidic devices.^[30]

Figure 4b presents the evolution of the integrated areas of the transitions depicted in Figure 4a, showing for T < 75 K an increase of I₂ at the cost of I₁. The temperature dependence of the Tb³⁺-to-Eu³⁺ energy transfer, occurring mainly via the dipole-quadrupole and quadrupole-quadrupole mechanisms,^[31] is a clear signature of a two-step concerted temperature-assisted energy transfer, as reported for Eu³⁺/Tb³⁺ co-doped di-ureasil organic-inorganic hybrids.^[30] Further insight into the energy-transfer mechanism is provided by the temperature dependence of the Δ parameter, which is well-described by the classical Mott–Seitz model for a single non-radiative recombination channel (see details in the Supporting Information, Figure S8 and S9).^[32]

$$\Delta(T) \approx \frac{\Delta_0}{1 + \alpha \exp(-\Delta E / k_B T)} \quad (1)$$

where Δ_0 is the Δ parameter at $T = 0$ K, $\alpha = W_0/W_R$ the ratio between the non-radiative (W_0 at $T = 0$ K) and radiative (W_R) rates, and ΔE the activation energy for the non-radiative channel (Figure. S9). The solid line in Figure 4c and in Figure S9 is the temperature calibration curve, obtained by fitting the experimental points to **Equation 1** ($r^2 > 0.9996$), yielding $\Delta_0 = 0.67 \pm 0.01$, $\alpha = 19.9 \pm 3.7$ and $\Delta E = 52.4 \pm 2.0$ cm⁻¹. According to the emission spectra of bulk and spray-drying prepared Tb_{0.9}Eu_{0.1}-PDA (recorded at room temperature and 12 K, Figure 3), this non-radiative channel involves deactivation through the ligand levels, whose broad emission overlaps the ⁵D₄ state.

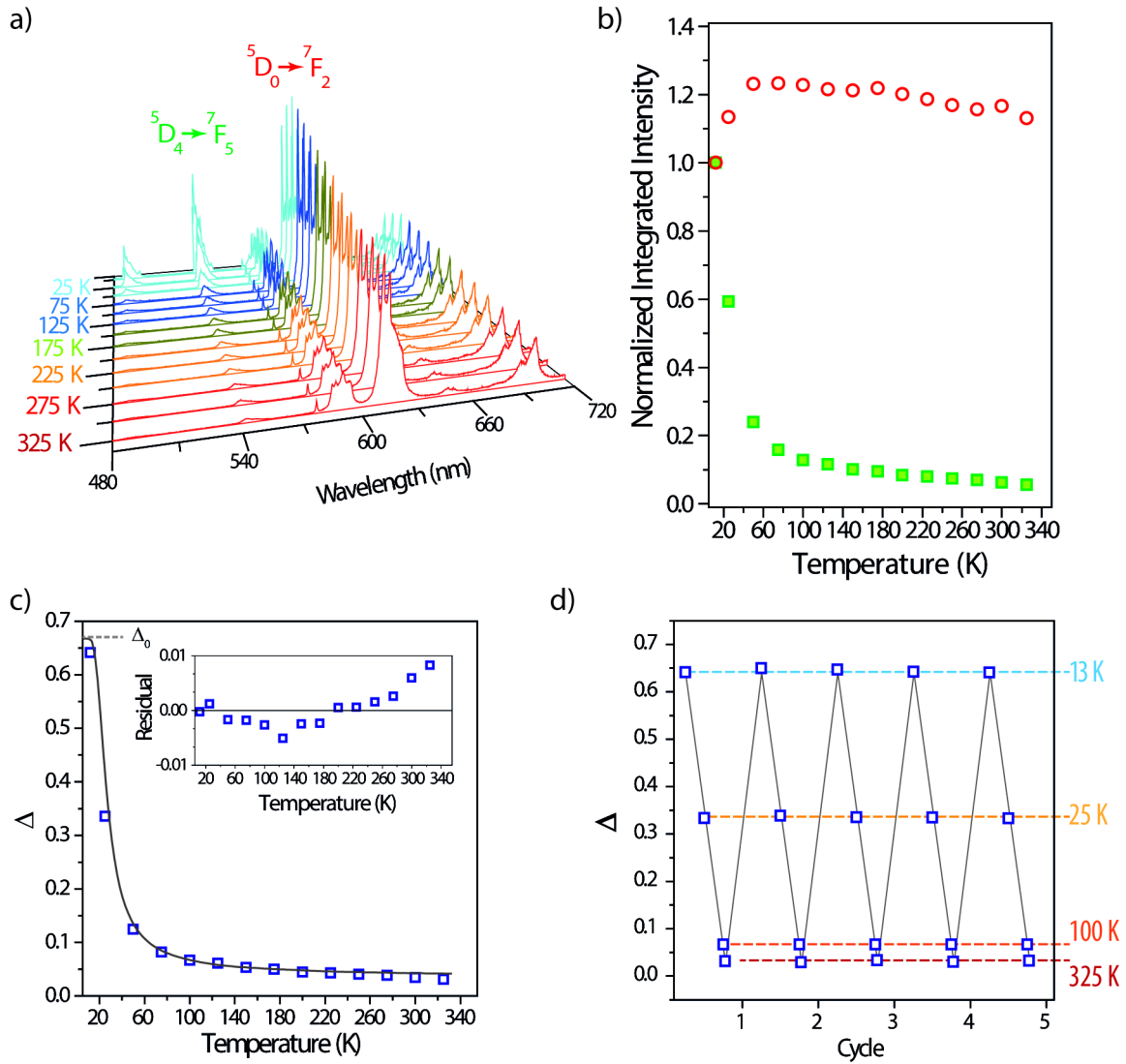


Figure 4. a) Emission spectra (excited at 377 nm, 10-325 K) of the spray-drying prepared MOF; b) I_1 (green) and I_2 (red) integrated areas; c) calibration curve. The open points depict the experimental Δ parameter and the solid line is the best fit to the experimental points ($r^2 >$

0.999) using Equation 1; the inset shows the residuals of the fit; d) temperature cycling between 13 and 325 K reveals reproducibility better than 99%.

The repeatability of the thermometer was measured over 5 consecutive temperature cycles between 13 and 325 K (Figure 4d and Figure S10); it was found that Δ is fully reversible without significant hysteresis, with repeatability better than 99%.

The thermometric performance is measured by the relative sensitivity, defined as:

$$S_r = \frac{\partial \Delta}{\partial T} / \Delta, \quad (2)$$

which is the figure of merit normally used to compare thermometers, irrespective of their nature.^[1a] **Figure 5a** depicts the temperature dependence of the relative sensitivity of spray-drying prepared Tb_{0.914}Eu_{0.086}-PDA in the range 10–325 K. The maximum sensitivity value of $5.96 \pm 0.04 \text{ \%} \cdot \text{K}^{-1}$ attained at 25 K is, to the best of our knowledge, the highest one reported in the cryogenic range (< 100 K) for luminescent thermometers, in particular when compared with the: (i) Eu/Tb-based MOF nanothermometers of Cui *et al.*,^[20-21] Cadiau *et al.*,^[22] Rao *et al.*,^[33] Zhou *et al.*,^[34] Wei *et al.*,^[35] Shen *et al.*,^[36] and Zhao *et al.*,^[37] which, although using distinct host matrices, adopt the same definition for the thermometric parameter; and (ii) the nanothermometers of D’Vries *et al.*,^[38] which take the ratio between I_1 (or I_2) and the broad triplet band intensity. Additionally, Figure 5a shows that, using distinct host matrices, Eu/Tb-based MOF nanothermometers cover the 10–340 K range with relative sensitivities in excess of $0.5 \text{ \%} \cdot \text{K}^{-1}$.

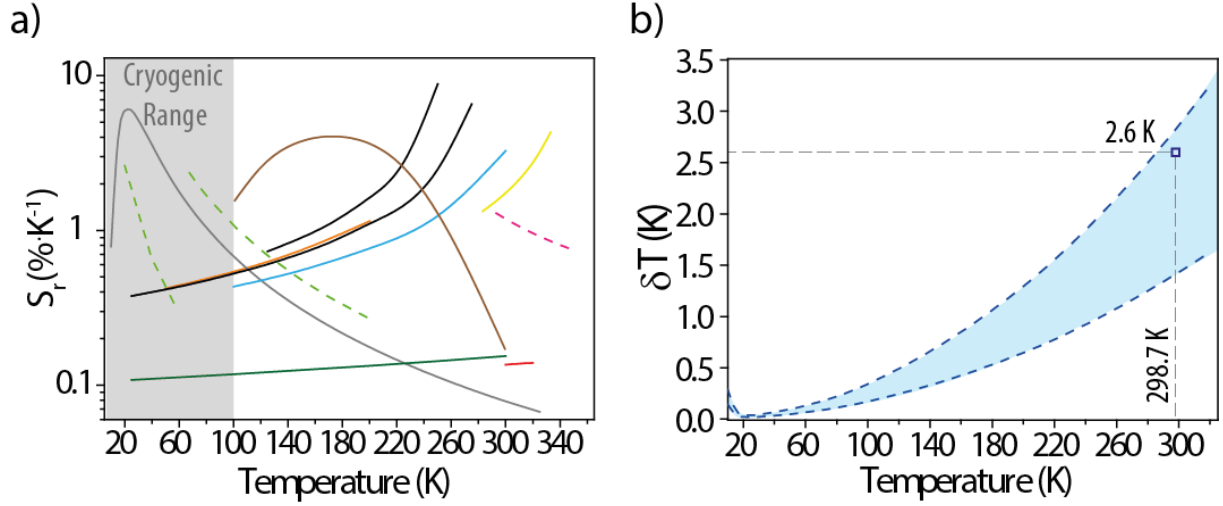


Figure 5. a) Relative sensitivity of the spray-drying prepared Tb_{0.914}Eu_{0.086}-PDA thermometer (gray line) ranging from 6.0 $\% \cdot K^{-1}$ (at 25 K) to 0.07 $\% \cdot K^{-1}$ (at 325 K). The relative sensitivities of the MOF thermometers reported by Cadiau *et al.*,^[22] (red), Cui *et al.*,^[20-21] (orange and pink), Rao *et al.*,^[33] (blue), D’Vries *et al.*,^[38] (green), Zhou *et al.*,^[34] (yellow), Wei *et al.*,^[35] (black) Shen *et al.*,^[36] (brown) and Zhao *et al.*^[37] (dark green) are also represented, for comparison. The solid lines are used for those thermometers whose thermometric parameter is defined as I_1/I_2 , whereas the dashed lines are used for other thermometers whose thermometric parameter is defined as the integrated intensity ratio between I_1 (or I_2) and the broad triplet band intensity,^[38] or as the ratio between I_2 and the emission luminescent perylene dye^[21]. The cryogenic temperature range is shadowed. b) Temperature uncertainty estimated using Equation 3 (blue shadowed area) and measured experimentally (open point).

If the relative sensitivity allows comparing the performance of different materials, the temperature uncertainty, δT depends on the actual temperature resolvable by the material, and on the experimental detection setup, as follows:

$$\delta T = \frac{1}{S_r} \frac{\delta \Delta}{\Delta}, \quad (3)$$

where $\delta \Delta / \Delta$ is the relative error in the determination of the thermometric parameter (defined by the acquisition setup). The detector used presents a maximum signal-to-noise-ratio of 1:450, meaning that $\delta \Delta / \Delta$ ranges from 0.45% (at full signal) to 0.90% (at half signal). The shadowed blue area in Figure 5b highlights the upper and lower limits of the temperature

uncertainty computed using Equation 3 (10–325 K). The open square point is an experimental evaluation of the temperature uncertainty obtained by taking 240 consecutive emission spectra, at 365 nm excitation, at 299 K (measured with an external K-type thermocouple). The conversion to temperature of each spectrum gives a Gaussian distribution of temperatures centered at 298.7 K, with a standard deviation of 2.6 K, an estimation of the temperature uncertainty of the measurement (Figure S11). This experimental result validates the boundary values estimated with Equation 3.

Concerning potential applications of the nanothermometer, it is evident that the temperature of maximum sensitivity is in the cryogenic range, below 100 K, for which the estimated temperature uncertainty is as low as 0.02 K. Cryogenic-temperature sensing is crucial in many research and industrial fields, such as energy and space exploration. Historically, it has been accomplished with electronic probes (silicon and gallium arsenide diodes, platinum, germanium, ruthenium oxide and rhodium-iron resistance temperature detectors, thermocouples and capacitance sensors)^[39] presenting the well-known disadvantages of contact measurements. Optical temperature sensing in this range was reported using the deformation of reflecting structures (e.g. fiber Bragg Gratings^[40]). Although these optical approaches do not suffer from interference with high electro and magnetic fields, the sensitive region of the probe is typically in the centimeter range.^[41] As an example, another optical technique, the Rayleigh backscattering spectral shift by optical frequency-domain reflectometry, presents a sensitivity as high as 9 %·K⁻¹ at 77.6 K (with an uncertainty of 0.3 K); however, this is a complex technique operative only at meter-length scales above 77 K and requiring a complex data analysis.^[42]

3. Conclusion

The spray-drying method is a promising general route for preparing MOF nanoparticles in the gram-to-kilogram scale. The first example of Ln³⁺-bearing MOF nanoparticles prepared by

spray-drying, $[(\text{Tb}_{0.914}\text{Eu}_{0.086})_2(\text{PDA})_3(\text{H}_2\text{O})]\cdot 2\text{H}_2\text{O}$ (PDA = 1,4-phenylenediacetic acid), reported here exhibits a quantum yield (0.25) larger than that of the bulk counterpart (0.16) and, in contrast, no ligand emission. The performance of these Ln-MOF nanoparticles as intensity-based ratiometric nanothermometers was evaluated in the 10–325 K range. It was concluded that this is the most sensitive cryogenic nanothermometer reported to date, with a remarkable combination of high sensitivity (up to $5.96 \pm 0.04 \text{ \%}\cdot\text{K}^{-1}$ at 25 K), high reproducibility (> 97%, at room temperature) and low-temperature uncertainty (0.02 K at 25 K). The high-temperature sensitivity is a direct consequence of the Tb^{3+} -to- Eu^{3+} energy transfer, occurring mainly via the dipole-quadrupole and quadrupole-quadrupole mechanisms. Using the classical Mott model, we have demonstrated that this performance is consistent with a thermally-activated Tb^{3+} -to-ligand energy back transfer mechanism, namely, a single non-radiative channel involving the deactivation of the $^5\text{D}_4$ level via the ligands.

4. Experimental Section

Spray-drying synthesis: Nanoparticles of $\text{Tb}_{0.914}\text{Eu}_{0.086}$ -PDA were synthesized using the spray-drying method, as previously described.^[24] Typically, a clear solution was prepared by dissolving $\text{Tb}(\text{NO}_3)_3\cdot 6\text{H}_2\text{O}$ (2.0 g, 99.9%, Aldrich), $\text{Eu}(\text{NO}_3)_3\cdot 5\text{H}_2\text{O}$ (0.21 g, 99.9%, Aldrich) and 1,4-phenylenediacetic acid (1.49 g, 97%, Alfa Aesar) in a mixture of dimethylformamide (DMF, 99%, Alfa Aesar) and water (350 mL, 50:50, vol%). The solution was spray-dried in a Mini Spray Dryer B-290 (BÜCHI Labortechnik) at a feed rate of 4.5 mL min^{-1} , flow rate of 336 mL min^{-1} and an inlet temperature of 453 K, using a two-fluid nozzle with a 0.5-mm-diameter hole. A white powder was collected and then washed with DMF, deionized water and acetone. The final product was dried at 363 K for 12 h. The yield was ca. 55%.

Synthesis of the bulk material: The bulk MOF material was prepared by the solvothermal method. 1,4-phenylenediacetic acid (85 mg, 97%, Alfa Aesar) was dissolved in DMF (5 mL) and $\text{Tb}(\text{NO}_3)_3$ aqueous solution (0.653 mL, 0.4 M), $\text{Eu}(\text{NO}_3)_3$ aqueous solution (0.058 mL, 0.5

m) and deionized water (5 mL) were added subsequently. The resulting solution was transferred into a 30 mL Teflon-lined autoclave. The synthesis was carried out in a convection oven heated at 403 K for 4 days. Light yellow crystals were recovered by filtration and washed thoroughly with DMF, deionized water and acetone. The same synthesis conditions were applied to prepare isostructural materials with a single metal, i.e. Y, Tb and Eu.

Photoluminescence Measurements: The luminescence spectra were recorded with a modular double grating excitation spectrofluorimeter with a TRIAX 320 emission monochromator (Fluorolog-3, Horiba Scientific) coupled to a R928 Hamamatsu photomultiplier, using the front face acquisition mode. The excitation source was a 450W Xe arc lamp. The emission spectra were corrected for the detection and optical spectral response of the spectrofluorimeter, while the excitation spectra were corrected for the spectral distribution of the lamp intensity using a photodiode reference detector. The temperature-dependent photoluminescence measurements were performed using a He closed-cycle cryostat, and the temperature (10–325 K, with a maximum accuracy of 0.1 K) was increased with a Lakeshore 331 auto-tuning temperature controller with a resistance heater. Temperature calibration of the nanosized MOF: the sample temperature was fixed to a particular value using the auto-tuning temperature controller; after waiting 5 minutes to thermalize the sample, the steady state emission spectrum of the samples was measured; the maximum temperature difference detected during the acquisitions was 0.1 K, the temperature accuracy of the controller; the emission spectrum was converted to temperature through the thermometric parameter

$\Delta = I_1 / I_2$ [30], where I_1 and I_2 are, respectively, the integrated areas of the $\text{Tb}^{3+} \ ^5\text{D}_4 \rightarrow \ ^7\text{F}_5$ and $\text{Eu}^{3+} \ ^5\text{D}_0 \rightarrow \ ^7\text{F}_2$ transitions.

The setup used to perform the temperature cycling and evaluating the uncertainty consisted of an excitation LED light source (LLS-365, Ocean Optics, 365 nm) connected to the outer fiber bundle (modified Ocean Optics QR450-7-XSR fiber). The emission was collected through the

central fiber and measured with a MAYA2000 PRO portable spectrometer (Ocean Optics), controlled by MatLab® routines. The integration time was 0.250 s.

Absolute Emission Quantum Yields: The absolute emission quantum yields were measured at room temperature using a C9920-02 system from Hamamatsu with a 150 W xenon lamp coupled to a monochromator for wavelength discrimination, an integrating sphere as sample chamber, and a multi-channel analyzer for signal detection. Three measurements were made for each sample and the average value is reported. The method is accurate within 10%.

Supporting Information

Supporting Information is available from the Wiley Online Library or from the author

Acknowledgements

This work was developed in the scope of the project CICECO-Aveiro Institute of Materials (Ref. FCT UID /CTM /50011/2013), financed by national funds through the FCT/MEC and when applicable co-financed by FEDER under the PT2020 Partnership Agreement. CDSB (SFRH/BPD/89003/2012) and DA (SFRH/BPD/95032/2013) thank FCT (Fundação para a Ciência e a Tecnologia) for post-doctoral grants. ZW also thanks the post-doctoral scholarship under the Project CENTRO-07-ST24-FEDER-002032. This work was also supported by the MINECO-Spain under the project PN MAT2012-30994 and EU FP7 ERC-Co 615954. I.I. thanks the MINECO for the RyC fellowship. ICN2 acknowledges support of the Spanish MINECO through the Severo Ochoa Centers of Excellence Program under Grant SEV-2013-0295.

References

- [1] a) C. D. S. Brites, P. P. Lima, N. J. O. Silva, A. Millan, V. S. Amaral, F. Palacio, L. D. Carlos, *Nanoscale* **2012**, 4, 4799; b) L. H. Fischer, G. S. Harms, O. S. Wolfbeis, *Angew. Chem. Int. Ed.* **2011**, 50, 4546; c) D. Jaque, F. Vetrone, *Nanoscale* **2012**, 4, 4301.
- [2] a) J. Lee, N. A. Kotov, *Nano Today* **2007**, 2, 48; b) S. Sadat, A. Tan, Y. J. Chua, P. Reddy, *Nano Lett.* **2010**, 10, 2613.
- [3] G. A. Baker, S. N. Baker, T. M. McCleskey, *Chem. Commun.* **2003**, 2932.
- [4] a) C.-Y. Chen, C.-T. Chen, *Chem. Commun.* **2011**, 47, 994; b) F. Ye, C. Wu, Y. Jin, Y.-H. Chan, X. Zhang, D. T. Chiu, *J. Am. Chem. Soc.* **2011**, 133, 8146; c) K. Okabe, N. Inada, C. Gota, Y. Harada, T. Funatsu, S. Uchiyama, *Nat. Commun.* **2012**, 3, 705.
- [5] a) E. J. McLaurin, V. A. Vlaskin, D. R. Gamelin, *J. Am. Chem. Soc.* **2011**, 133, 14978; b) C.-H. Hsia, A. Wuttig, H. Yang, *ACS Nano* **2011**, 5, 9511; c) A. E. Albers, E. M. Chan, P. M. McBride, C. M. Ajo-Franklin, B. E. Cohen, B. A. Helms, *J. Am. Chem. Soc.* **2012**, 134, 9565; d) S. L. Shinde, K. K. Nanda, *Angew. Chem. Int. Ed.* **2013**, 52, 11325.
- [6] a) C. D. S. Brites, P. P. Lima, N. J. O. Silva, A. Millan, V. S. Amaral, F. Palacio, L. D. Carlos, *New J. Chem.* **2011**, 35, 1177; b) L. D. Carlos, R. A. S. Ferreira, V. de Zea Bermudez, B. Julian-Lopez, P. Escribano, *Chem. Soc. Rev.* **2011**, 40, 536.
- [7] E. Saïdi, B. Samson, L. Aigouy, S. Volz, P. Löw, C. Bergaud, M. Mortier, *Nanotechnology* **2009**, 20, 115703.
- [8] L. Aigouy, E. Saidi, L. Lalouat, J. Labeguerie-Egea, M. Mortier, P. Low, C. Bergaud, *J. Appl. Phys.* **2009**, 106, 074301.
- [9] F. Vetrone, R. Naccache, A. Zamarrón, A. Juarranz de la Fuente, F. Sanz-Rodríguez, L. Martinez Maestro, E. Martín Rodriguez, D. Jaque, J. García Solé, J. A. Capobianco, *ACS Nano* **2010**, 4, 3254.
- [10] S. Zheng, W. Chen, D. Tan, J. Zhou, Q. Guo, W. Jiang, C. Xu, X. Liu, J. Qiu, *Nanoscale* **2014**, 6, 5675.

- [11] A. H. Khalid, K. Kontis, *Meas. Sci. Technol.* **2009**, *20*, 025305.
- [12] S. W. Allison, G. T. Gillies, A. J. Rondinone, M. R. Cates, *Nanotechnology* **2003**, *14*, 859.
- [13] B. Dong, B. Cao, Y. He, Z. Liu, Z. Li, Z. Feng, *Adv. Mater.* **2012**, *24*, 1987.
- [14] H. Peng, M. I. J. Stich, J. Yu, L.-n. Sun, L. H. Fischer, O. S. Wolfbeis, *Adv. Mater.* **2010**, *22*, 716.
- [15] C. D. S. Brites, P. P. Lima, N. J. O. Silva, A. Millán, V. S. Amaral, F. Palacio, L. D. Carlos, *Adv. Mater.* **2010**, *22*, 4499.
- [16] a) M. D. Allendorf, C. A. Bauer, R. K. Bhakta, R. J. T. Houk, *Chem. Soc. Rev.* **2009**, *38*, 1330; b) J. Rocha, L. D. Carlos, F. A. A. Paz, D. Ananias, *Chem. Soc. Rev.* **2011**, *40*, 926.
- [17] C. Serre, F. Millange, C. Thouvenot, N. Gardant, F. Pelle, G. Ferey, *J. Mater. Chem.* **2004**, *14*, 1540.
- [18] a) L. E. Kreno, K. Leong, O. K. Farha, M. Allendorf, R. P. Van Duyne, J. T. Hupp, *Chem. Rev.* **2012**, *112*, 1105; b) Y. Takashima, V. M. Martínez, S. Furukawa, M. Kondo, S. Shimomura, H. Uehara, M. Nakahama, K. Sugimoto, S. Kitagawa, *Nat. Commun.* **2011**, *2*, 168; c) B. V. Harbuzaru, A. Corma, F. Rey, P. Atienzar, J. L. Jordá, H. García, D. Ananias, L. D. Carlos, J. Rocha, *Angew. Chem. Int. Ed.* **2008**, *47*, 1080; d) Y. Cui, Y. Yue, G. Qian, B. Chen, *Chem. Rev.* **2012**, *112*, 1126; e) B. V. Harbuzaru, A. Corma, F. Rey, J. L. Jordá, D. Ananias, L. D. Carlos, J. Rocha, *Angew. Chem. Int. Ed.* **2009**, *48*, 6476.
- [19] a) W. J. Rieter, K. M. Pott, K. M. L. Taylor, W. Lin, *J. Am. Chem. Soc.* **2008**, *130*, 11584; b) H. Xu, F. Liu, Y. Cui, B. Chen, G. Qian, *Chem. Commun.* **2011**, *47*, 3153; c) J. Della Rocca, D. Liu, W. Lin, *Acc. Chem. Res.* **2011**, *44*, 957; d) W. Yang, J. Feng, H. Zhang, *J. Mater. Chem.* **2012**, *22*, 6819.
- [20] Y. Cui, H. Xu, Y. Yue, Z. Guo, J. Yu, Z. Chen, J. Gao, Y. Yang, G. Qian, B. Chen, *J. Am. Chem. Soc.* **2012**, *134*, 3979.

- [21] Y. Cui, R. Song, J. Yu, M. Liu, Z. Wang, C. Wu, Y. Yang, Z. Wang, B. Chen, G. Qian, *Adv. Mater.* **2015**, 27, 1420.
- [22] A. Cadiau, C. D. S. Brites, P. M. F. J. Costa, R. A. S. Ferreira, J. Rocha, L. D. Carlos, *ACS Nano* **2013**, 7, 7213.
- [23] E. A. Flugel, A. Ranft, F. Haase, B. V. Lotsch, *J. Mater. Chem.* **2012**, 22, 10119.
- [24] A. Carné-Sánchez, I. Imaz, M. Cano-Sarabia, D. Maspoch, *Nat. Chem.* **2013**, 5, 203.
- [25] A. G. Marquez, P. Horcajada, D. Grosso, G. Ferey, C. Serre, C. Sanchez, C. Boissiere, *Chem. Commun.* **2013**, 49, 3848.
- [26] L. Pan, K. M. Adams, H. E. Hernandez, X. Wang, C. Zheng, Y. Hattori, K. Kaneko, *J. Am. Chem. Soc.* **2003**, 125, 3062.
- [27] Y.-W. Ren, J.-X. Liang, J.-X. Lu, B.-W. Cai, D.-B. Shi, C.-R. Qi, H.-F. Jiang, J. Chen, D. Zheng, *Eur. J. Inorg. Chem.* **2011**, 2011, 4369.
- [28] W. Carnall, H. Crosswhite, H. M. Crosswhite, *Energy level structure and transition probabilities in the spectra of the trivalent lanthanides in LaF₃*, Argonne National Lab., IL (USA), **1978**.
- [29] a) C. D. S. Brites, P. P. Lima, N. J. O. Silva, A. Millán, V. S. Amaral, F. Palacio, L. D. Carlos, *J. Lumin.* **2013**, 133, 230; b) R. A. S. Ferreira, C. D. S. Brites, C. M. S. Vicente, P. P. Lima, A. R. N. Bastos, P. G. Marques, M. Hiltunen, L. D. Carlos, P. S. André, *Laser Photon. Rev.* **2013**, 7, 1027.
- [30] C. D. S. Brites, P. P. Lima, N. J. O. Silva, A. Millan, V. S. Amaral, F. Palacio, L. D. Carlos, *Nanoscale* **2013**, 5, 7572.
- [31] C. V. Rodrigues, L. L. Luz, J. D. L. Dutra, S. A. Junior, O. L. Malta, C. C. Gatto, H. C. Streit, R. O. Freire, C. Wickleder, M. O. Rodrigues, *PCCP* **2014**, 16, 14858.
- [32] a) N. F. Mott, *Proceedings of the Royal Society of London A: Mathematical, Physical and Engineering Sciences* **1938**, 167, 384; b) F. Seitz, *Transactions of the Faraday Society* **1939**, 35, 74.

- [33] X. Rao, T. Song, J. Gao, Y. Cui, Y. Yang, C. Wu, B. Chen, G. Qian, *J. Am. Chem. Soc.* **2013**, *135*, 15559.
- [34] Y. Zhou, B. Yan, F. Lei, *Chem. Commun.* **2014**, *50*, 15235.
- [35] Y. Wei, R. Sa, Q. Li, K. Wu, *Dalton Trans* **2015**, *44*, 3067.
- [36] X. Shen, Y. Lu, B. Yan, *Eur. J. Inorg. Chem.* **2015**, *2015*, 916.
- [37] S.-N. Zhao, L.-J. Li, X.-Z. Song, M. Zhu, Z.-M. Hao, X. Meng, L.-L. Wu, J. Feng, S.-Y. Song, C. Wang, H.-J. Zhang, *Adv. Funct. Mater.* **2015**, *25*, 1463.
- [38] R. F. D'Vries, S. Alvarez-Garcia, N. Snejko, L. E. Bausa, E. Gutierrez-Puebla, A. de Andres, M. A. Monge, *J. Mater. Chem. C* **2013**, *1*, 6316.
- [39] a) J. Ylöstalo, P. Berglund, O. Niinikoski, R. Voutilainen, *Cryogenics* **1996**, *36*, 1033;
b) R. L. Rusby, M. Kempson, *Rev. Gen. Therm.* **1996**, *35*, 338.
- [40] Z.-S. Guo, J. Feng, H. Wang, *Cryogenics* **2012**, *52*, 457.
- [41] V. K. Rai, *Appl. Phys. B* **2007**, *88*, 297.
- [42] Y. Du, T. Liu, Z. Ding, Q. Han, K. Liu, J. Jiang, Q. Chen, B. Feng, *Photonics Technology Letters, IEEE* **2014**, *26*, 1150.

One of the most sensitive cryogenic thermometers ($5.96\% \cdot \text{K}^{-1}$ at 25 K) reported so far is described, consisting of lanthanide (Tb^{3+} , Eu^{3+}) organic framework nanoparticles prepared by spray-drying, exhibiting an excellent reproducibility ($> 99\%$) and low-temperature uncertainty (0.02 K at 25 K).

MOFs, Lanthanides, spray-drying, luminescence, thermometers

Z. Wang, D. Ananias, A. Carné-Sánchez, C. D. S. Brites, I. Imaz, D. MasPOCH, J. Rocha* and L. D. Carlos*

Lanthanide Organic Framework Nanothermometers Prepared by Spray-Drying

